ECS Transactions, 58 (35) 21-32 (2014)
10.1149/05835.0021ecst ©The Electrochemical Society

Understanding Chlorite, Chlorate and Perchlorate Formation When Generating Hypochlorite Using Boron Doped Diamond Film Electrodes

D. K. Hubler[a], J. C. Baygents[a], B. P. Chaplin[b], J. Farrell[a]

[a] Department of Chemical and Environmental Engineering, University of Arizona, Tucson, Arizona 85721, USA
[b] Department of Chemical Engineering, University of Illinois at Chicago, Chicago, Illinois 60607, USA

This research used density functional theory for investigating reactions on boron doped diamond (BDD) film electrodes that contribute to unwanted byproduct formation during hypochlorite generation. Clusters containing 10 carbon atoms were used to simulate the diamond electrode surface. The simulations included reactions with hydrogen terminated surfaces, and with surface sites produced by anodic polarization, namely: ≡C$^{\bullet}$, =C$^{\bullet}$H, ≡C-O$^{\bullet}$ and =C$^{\bullet}$HO. The activation energies for oxidation of chlorine oxyanions via direct electron transfer and via reaction with hydroxyl radicals were calculated. Oxychlorine radicals ($ClO^{\bullet}$, $ClO_2^{\bullet}$, $ClO_3^{\bullet}$) were found to chemically adsorb to both secondary and tertiary carbon atoms on the BDD surface. These chemisorbed intermediates could react with hydroxyl radicals to regenerate the original chlorine oxyanion (ClO^-, ClO_2^-, ClO_3^-), and produce ≡C-O$^{\bullet}$ and =C$^{\bullet}$HO sites on the BDD surface. The ≡C-O$^{\bullet}$ and =C$^{\bullet}$HO sites also reacted with oxychlorine radicals to form chemisorbed intermediates, which could then be converted to higher oxidation states (ClO_2^-, ClO_3^-, ClO_4^-) via reaction with hydroxyl radicals.

Introduction

Boron-doped diamond (BDD) electrodes are seeing increased use in water treatment applications due to their chemical stability and effectiveness in oxidizing a wide variety of organic and inorganic compounds. The oxidizing power of BDD anodes stems from their high overpotential for oxygen evolution (1). This feature allows BDD anodes to be polarized to high potentials in aqueous systems while still maintaining high Faradaic current efficiencies for target compound oxidation. Oxidation of compounds by BDD anodes has been found to occur via both direct electron transfer and hydroxyl radicals generated from water oxidation (2, 3, 4, 5, 6, 7).

One proposed use of BDD anodes is for on-site generation of hypochlorite in cooling tower, drinking water, or swimming pool applications (8). This is accomplished by oxidizing chloride ions (Cl^-) to hypochlorite ions (OCl^-) and hypochlorous acid (HOCl). Several studies have found significant quantities of chlorate (ClO_3^-) and perchlorate (ClO_4^-) may be produced when chloride solutions are electrolyzed (9, 10, 11, 12). All oxychlorine anions are present in electrolyzed chloride solutions, including hypochlorite, chlorite (ClO_2^-), chlorate and perchlorate. Batch experiments show complete conversion of chloride to perchlorate can be achieved with prolonged electrolysis times. Perchlorate production can be minimized in batch and flow-through systems by using low current

densities, high mass transfer rates, and high concentrations of chloride (9, 11, 12). High mass transfer rates, driven by fluid convection, are hypothesized to affect the multistep reaction for perchlorate formation from chloride, as chloride ions are progressively oxidized to higher oxychlorine anions, as illustrated by:

$$Cl^- \rightarrow OCl^- \rightarrow ClO_2^- \rightarrow ClO_3^- \rightarrow ClO_4^- \quad [1]$$

High rates of mass transfer near the surface result in low concentrations of intermediate products, so that complete chloride oxidation to perchlorate can be minimized.

The production of perchlorate during electrolysis is problematic due to its carcinogenic potential and its adverse effects on thyroid gland function (13, 14, 15). These health risks have prompted the United States Environmental Protection Agency to issue an advisory target of 15 µg/L for perchlorate in drinking water (16). Furthermore, two states, California and Massachusetts, have mandated even lower drinking water limits for perchlorate of 6 and 2 µg/L, respectively (17, 18).

The goal of this research was to use density functional theory (DFT) simulations to develop plausible reaction pathways for oxidizing OCl^- to ClO_4^- at BDD anodes. Direct electron transfer reactions were modeled for generating hydroxyl ($HO^\bullet$) and $ClO_x^\bullet$ radicals. Additionally, reactions of these species with each other and with sites on the BDD surface were investigated. Mechanisms in which $ClO_x^\bullet$ radicals chemisorb to the anode surface were also considered, and several reaction pathways between Cl^- and ClO_4^- were elucidated.

Materials and Methods

Simulation Cluster

The hydrogen terminated 10-carbon atom cluster shown in Figure 1 was used to model the electrode surface. In addition to simulations using this hydrogen terminated structure, simulations were also performed using functional groups produced by anodic polarization of the electrodes.

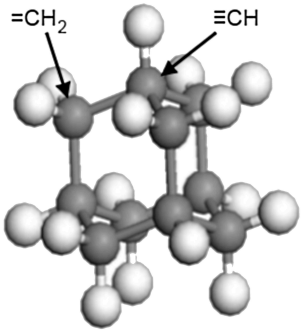

Figure 1. 10-carbon structure used for simulating the diamond surface. The structure is $C_{10}H_{16}$, and the surface has both ≡CH sites and $=CH_2$ sites. Atom key: carbon, grey; hydrogen, white.

Freshly prepared BDD surfaces are terminated with hydrogen atoms (19, 20, 21, 22). However, anodic polarization results in oxidation of the surface to produce carboxyl (≡C-

OH), carbonyl (=C=O), and aldehyde (=CHO) functional groups. These functional groups have a major effect on the physical, chemical and electronic characteristics of the BDD surface, and impact the mechanism of both anodic and cathodic reactions (4, 5, 23). These functional groups may also become oxidized themselves under anodic polarization, and anodically polarized BDD surfaces are believed to contain carbon radical (≡C$^{\bullet}$), carboxyl radical (≡C-O$^{\bullet}$), and aldehyde radical (=CH-O$^{\bullet}$) functional groups (24). Therefore, simulations were also performed using oxygen and carbon radical terminated surfaces.

DFT Methods

All DFT calculations were performed with the DMol3 package in the Accelrys Materials Studio modeling suite on a personal computer (25, 26, 27). All simulations used double-numeric with polarization (DNP) basis sets and the gradient-corrected Becke-Lee-Yang-Parr (BLYP) functionals for exchange and correlation (28, 29, 30). The nuclei and core electrons were described by DFT optimized semilocal pseudopotentials (31). Implicit solvation was incorporated into all simulations by use of the COSMO-ibs polarizable continuum model (32). Thermal smearing of 0.005 Ha was used to facilitate numerical convergence. The reaction energies (ΔE) presented here represent the 0 K reaction energies without thermal or zero-point corrections. These corrections are small (< 4 kJ/mol) and are less than the errors in the calculation of the reaction energies themselves, which may be up to 16 kJ/mol (33).

The activation energies (E_a) for direct electron transfer as a function of the electrode potential were calculated by the method of Anderson and Kang (34, 35). Reactant energies were calculated as a function of the reaction coordinate, defined as the bond length of the bond that was formed or broken during the reaction. Product energies were calculated using the atomic positions determined from the optimized reactant structures, followed by self-consistent field optimization of the electronic configurations. The energy of the free electron on the vacuum scale was adjusted to the standard hydrogen electrode (SHE) scale by subtracting 4.6 eV (34). Product energies were adjusted to reflect the electrode potential by shifting the energy profile of the product species downwards by 96.5 kJ/mol (i.e., 1.0 eV) to increase the electrode potential by 1.0 V and upwards by 96.5 kJ/mol to decrease the electrode potential by 1.0 V. Intersection of the product and reactant energy profiles yields the bond length of transition state and the activation energy for the reaction (34). Simulations involving solvated protons included two explicit water molecules to more accurately mimic physical reality (36).

Results and Discussion

Chlorite Formation

DFT simulations were used to investigate reaction mechanisms for ClO_2^- and $HClO_2$ formation starting from OCl^- or HOCl. Since BDD anodes are known to generate hydroxyl radicals, reactions of HO$^{\bullet}$ with OCl^- and HOCl in homogeneous solution were considered. The $HClO_2^-$ structure formed by combining HO$^{\bullet}$ with OCl^- was found to be unstable, and thus this reaction does not occur. However, reaction of HO$^{\bullet}$ with HOCl is a route for production of the OCl$^{\bullet}$ species via the reaction:

$$HOCl + HO^{\bullet} \rightarrow OCl^{\bullet} + H_2O \quad [2]$$

This reaction is activationless and has a reaction energy of $\Delta E = -127$ kJ/mol. The hypochlorite radical ($OCl^{\bullet}$) may also be produced via direct electron transfer from HOCl to the electrode via the reaction:

$$HOCl \rightarrow [HOCl]^{+} + e^{-} \rightarrow OCl^{\bullet} + H^{+} + e^{-} \quad [3]$$

Figure 2 shows the activation energy for reaction [3] as a function of electrode potential. At room temperature, this reaction should begin to happen at measurable rates at potentials above ~1.9 V/SHE (where the E_a drops below 40 kJ/mol), and the reaction becomes activationless at potentials above 2.36 V/SHE.

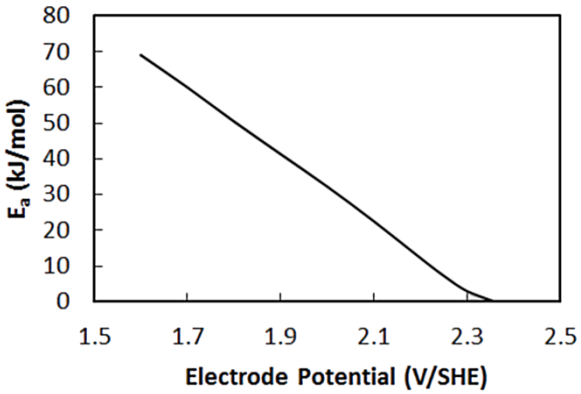

Figure 2. Activation energy as a function of electrode potential for reaction (3).

Both $HO^{\bullet}$ and $OCl^{\bullet}$ radicals are present in the solution near the electrode surface, so the combination of the two radicals to form $HClO_2$ was considered, as in the following reaction:

$$OCl^{\bullet} + HO^{\bullet} \rightarrow HClO_2 \quad [4]$$

Reaction [4] is activationless with a reaction energy $\Delta E = -90$ kJ/mol.

Additional DFT simulations were conducted to investigate the role of oxidized surface sites in the production of chlorite. These simulations considered the interaction of $OCl^{\bullet}$ with four oxidized surface sites, shown across the top of Figure 3, which shows production pathways for $HClO_2$, starting with $OCl^{\bullet}$ and $HO^{\bullet}$.

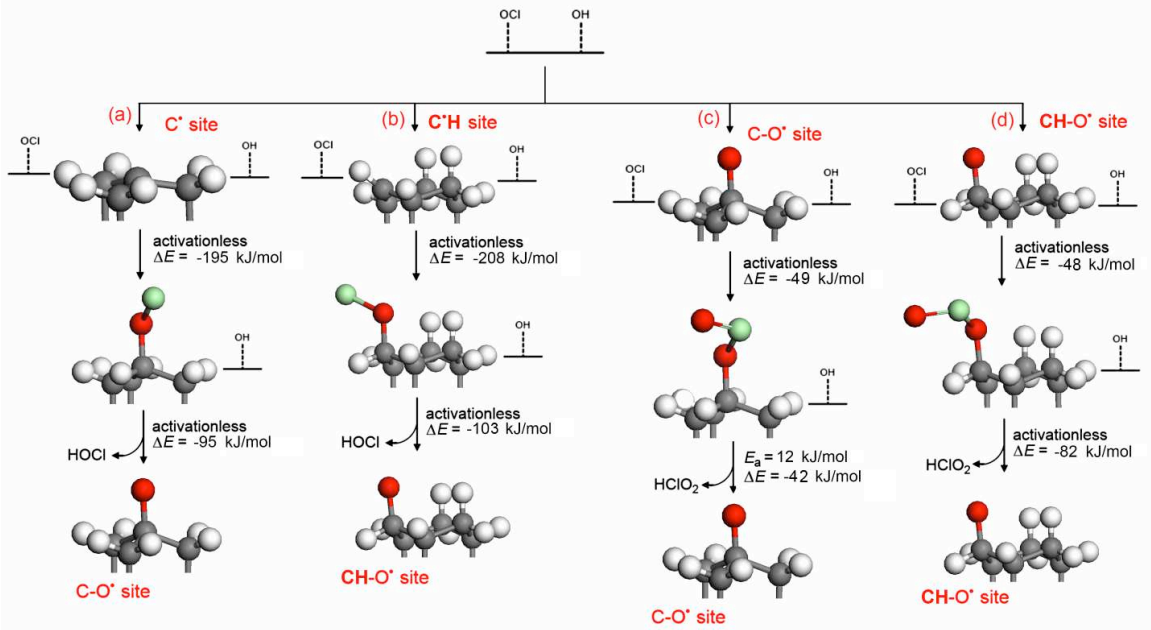

Figure 3. Scheme for OCl• interaction at oxidized diamond surface sites, including (a) ≡C• site, (b) =C•H site, (c) ≡C-O• site, and (d) ≡CH-O• site. Atom key for electronic version of manuscript: carbon, grey; hydrogen, white; oxygen, red; chlorine, green.

The ≡C• site and ≡C-O• site in (a) and (c) of Figure 3 are typical sp^3 carbon radical sites in which the carbon atom has bonds to three other carbon atoms. The =C•H site and ≡CH-O• site in (b) and (d) show a carbon atom with bonds to two other carbon atoms. This site may occur at the edge of a crystal in the polycrystalline BDD surface.

Figure 3(a) illustrates a two-step scheme for oxidation of a ≡C• site in the presence of hypochlorite radicals:

$$\equiv C^{\bullet} + OCl^{\bullet} \rightarrow \equiv C\text{-}OCl \qquad [5]$$

$$\equiv C\text{-}OCl + HO^{\bullet} \rightarrow \equiv C\text{-}O^{\bullet} + HOCl \qquad [6]$$

Both steps are activationless, with $\Delta E = -195$ kJ/mol for reaction [5] and $\Delta E = -95$ kJ/mol for reaction [6].

Figure 3(b) illustrates a two-step scheme for oxidation of an edge ≡C•H site in the presence of hypochlorite radicals:

$$=C^{\bullet}H + OCl^{\bullet} \rightarrow =CH\text{-}OCl \qquad [7]$$

$$=CH\text{-}OCl + HO^{\bullet} \rightarrow =CH\text{-}O^{\bullet} + HOCl. \qquad [8]$$

Both steps are activationless, with $\Delta E = -208$ kJ/mol for reaction [7] and $\Delta E = -103$ kJ/mol for reaction [8].

Once oxidized, the sites may catalyze $HClO_2$ production. Figure 3(c) shows a two-step scheme for chlorite production at a ≡C-O• site:

$$\equiv C\text{-}O^{\bullet} + OCl^{\bullet} \rightarrow \equiv C\text{-}O\text{-}ClO \quad [9]$$

$$\equiv C\text{-}O\text{-}ClO + HO^{\bullet} \rightarrow \equiv C\text{-}O^{\bullet} + HClO_2 \quad [10]$$

The chemisorption reaction is activationless with an energy change of $\Delta E = -49$ kJ/mol for reaction [9]. The subsequent oxidation step, reaction [10], has an activation energy of 12 kJ/mol and an overall energy change of $\Delta E = -42$ kJ/mol.

Similarly, Figure 3(d) shows a two-step scheme for chlorous acid production at the oxidized edge site:

$$=CH\text{-}O^{\bullet} + OCl^{\bullet} \rightarrow =CH\text{-}O\text{-}ClO \quad [11]$$

$$=CH\text{-}O\text{-}ClO + HO^{\bullet} \rightarrow =CH\text{-}O^{\bullet} + HClO_2 \quad [12]$$

Both steps are activationless, with $\Delta E = -48$ kJ/mol for reaction [11] and $\Delta E = -82$ kJ/mol for reaction [12].

In all cases, oxygen radical sites act catalytically in producing chlorous acid. These sites may be generated by reaction with $OCl^{\bullet}$ radicals, in which the oxygen attacks a carbon radical surface site. Carbon radical surface sites do not interact with the chlorine atoms of $OCl^{\bullet}$ radicals. The abundance of pathways that are activationless or require low activation energy suggests that the surface may be involved in ClO_2^- production by chemisorbing radical species, stabilizing them and giving them a longer lifetime. This increases the opportunity for $OCl^{\bullet}$ and $HO^{\bullet}$ to react.

Chlorate Formation

DFT simulations were used to investigate reaction mechanisms for ClO_3^- and $HClO_3$ production from ClO_2^- and $HClO_2$. Since BDD anodes are known to generate hydroxyl radicals, the combinations of $HO^{\bullet}$ with ClO_2^- and $HClO_2$ in homogeneous solution were considered. The $HClO_3^-$ structure formed by combining $HO^{\bullet}$ with ClO_2^- was found to be unstable, and thus this reaction does not occur. The reaction of $HO^{\bullet}$ with $HClO_2$ is a route for activationless production of $ClO_2^{\bullet}$ species via the reaction:

$$HClO_2 + HO^{\bullet} \rightarrow ClO_2^{\bullet} + H_2O \quad [13]$$

For reaction [13] the energy change is $\Delta E = -21$ kJ/mol.

$ClO_2^{\bullet}$ production may also occur via direct electron transfer from $HClO_2$ to the electrode. This occurs in the following reaction:

$$HClO_2 \rightarrow [HClO_2]^+ + e^- \rightarrow ClO_2^{\bullet} + H^+ + e^- \quad [14]$$

Figure 4 shows the activation energy for $HClO_2$ oxidation as a function of the electrode potential. The reaction will begin to occur at measurable rates at potentials above ~1.5 V/SHE, and becomes activationless at potentials above 2.10 V/SHE.

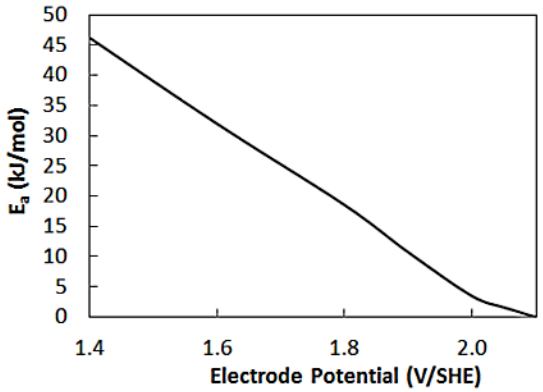

Figure 4. Activation energy as a function of electrode potential for reaction [14].

The $ClO_2^{\bullet}$ species generated in reactions [13] and [14] can react with $HO^{\bullet}$ to form $HClO_3$, as in the following reaction:

$$ClO_2^{\bullet} + HO^{\bullet} \rightarrow HClO_3 \quad [15]$$

This reaction is activationless with an energy change of $\Delta E = -142$ kJ/mol.

The interaction of $ClO_2^{\bullet}$ species with the surface was also considered. Figure 5 shows a scheme for $ClO_2^{\bullet}$ interactions with oxidized surface sites on boron-doped diamond anodes that result in $HClO_3$ production. In general, $ClO_2^{\bullet}$ can interact with carbon radical sites on the surface, resulting in formation of oxygen radical sites on the surface. Then, $ClO_2^{\bullet}$ can interact with the oxygen radical sites to produce $HClO_3$.

$ClO_2^{\bullet}$ chemisorbs to two types of carbon radical sites on the diamond surface, as in the following reactions:

$$\equiv C^{\bullet} + ClO_2^{\bullet} \rightarrow \equiv C\text{-}OClO \quad [16]$$

$$=C^{\bullet}H + ClO_2^{\bullet} \rightarrow =CH\text{-}OClO \quad [17]$$

Reactions [16] and [17] are both activationless, with an overall energy change of $\Delta E = -144$ kJ/mol for reaction [16], and $\Delta E = -156$ kJ/mol for reaction [17].

Each of these chemisorbed species will undergo $HO^{\bullet}$ attack, resulting in the oxygen radical surface sites shown in Figure 5(c) and (d). This attack regenerates the $HClO_2$ molecule, which then reacts with hydrogen terminated sites on the surface. This produces HOCl and $HO^{\bullet}$.

The chlorate radical also reacts with oxygen radical sites in the following reactions:

$$\equiv C\text{-}O^{\bullet} + ClO_2^{\bullet} \rightarrow \equiv C\text{-}O\text{-}ClO_2 \quad [18]$$

$$=CH\text{-}O^{\bullet} + ClO_2^{\bullet} \rightarrow =CH\text{-}O\text{-}ClO_2 \quad [19]$$

These reactions each require an activation energy, which is 9.1 kJ/mol for reaction [18] and 9.2 kJ/mol for reaction [19]. The energy changes for these reactions are $\Delta E = -39$ kJ/mol for reaction [18] and $\Delta E = -54$ kJ/mol for reaction [19].

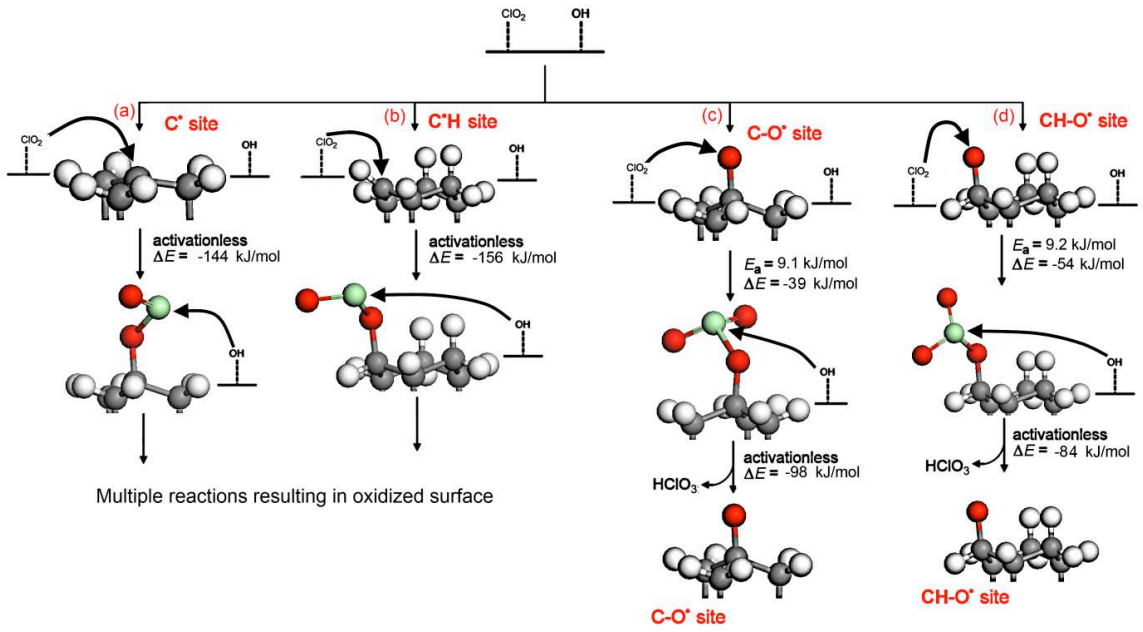

Figure 5. Scheme for $ClO_2^{\bullet}$ interaction with four sites on the bulk diamond surface: (a) $\equiv C^{\bullet}$, (b) $=C^{\bullet}H$, (c) $\equiv C\text{-}O^{\bullet}$, and (d) $=CH\text{-}O^{\bullet}$. Atom key for electronic version of manuscript: carbon, grey; hydrogen, white; oxygen, red; chlorine, green.

Each of these chemisorbed surface complexes may be attacked by an $HO^{\bullet}$ to yield $HClO_3$. These reactions are shown below:

$$\equiv C\text{-}O\text{-}ClO_2 + HO^{\bullet} \rightarrow \equiv C\text{-}O^{\bullet} + HClO_3 \quad [20]$$

$$=CH\text{-}O\text{-}ClO_2 + HO^{\bullet} \rightarrow =CH\text{-}O^{\bullet} + HClO_3 \quad [21]$$

Both reactions are activationless, with $\Delta E = -98$ kJ/mol for reaction [20], and $\Delta E = -83$ kJ/mol for reaction [21].

Perchlorate Formation

Production of perchlorate from chlorate has been presented previously in Azizi *et al.* (37). A brief summary of the most important reactions is contained here. Figure 6 shows the generation of $ClO_3^{\bullet}$ and $HO^{\bullet}$ near the BDD anode surface, which subsequently combine, activationlessly, to form $HClO_4$. Chlorate radical production occurs more readily than water oxidation, as it becomes activationless at 0.76 V/SHE. The combination of radicals is activationless, with a reaction energy $\Delta E = -133$ kJ/mol.

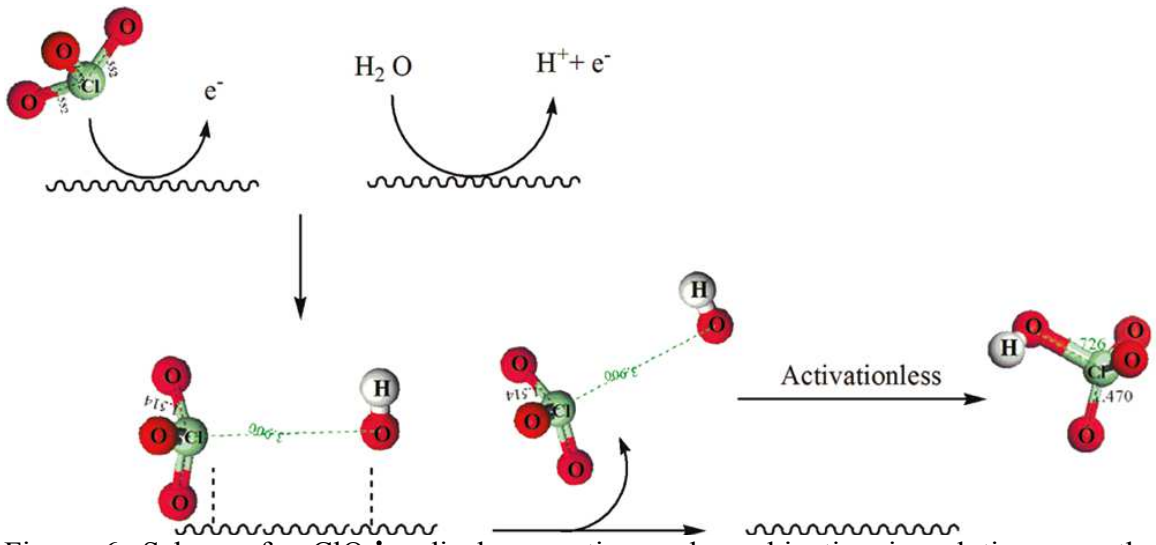

Figure 6. Scheme for $ClO_3^{\bullet}$ radical generation and combination in solution near the electrode surface to form $HClO_4$. Atom key for electronic version of manuscript: hydrogen, white; oxygen, red; chlorine, green.

Figure 7(a) illustrates two mechanisms for generating $HClO_3$ from $ClO_3^{\bullet}$ species chemisorbed at a $\equiv C^{\bullet}$ site via either chlorine or oxygen atoms. Attack by $HO^{\bullet}$ on the chemisorbed chlorate species produces $HClO_3$ and an oxygen radical site on the surface. The activation energies for these reactions of 27 and 13 kJ/mol are sufficiently low that these reactions should readily occur at room temperature.

Figure 7(b) shows the reactions of $ClO_3^{\bullet}$ at a $\equiv C\text{-}O^{\bullet}$ site. The direct reaction between $ClO_3^{\bullet}$ and a $\equiv C\text{-}O^{\bullet}$ site is activationless and produces O_2 and $HClO_2$. Attack by $HO^{\bullet}$ on the chlorine atom in the chemisorbed chlorate species produces $HClO_4$ as shown in the following reaction:

$$\equiv C\text{-}O\text{-}ClO_3 + HO^{\bullet} \rightarrow \equiv C\text{-}O^{\bullet} + HClO_4 \qquad [22]$$

The activation barrier for this reaction is 66 kJ/mol, and thus the rate of this reaction is expected to be low at room temperature.

Conclusion

This manuscript presents a plausible set of reaction pathways for producing perchlorate from hypochlorite using a BDD anode. Both protonated and unprotonated hypochlorite, chlorite and chlorate species can be oxidized to their respective radical, $ClO_x^{\bullet}$, at potentials below that for water oxidation. In addition, hypochlorous, chlorous and chloric acids can be oxidized by $HO^{\bullet}$ produced from water oxidation. The oxychlorine radical species may react with $HO^{\bullet}$ in solution to form a more oxidized species, or may chemisorb to anodically generated $\equiv C^{\bullet}$, $=C^{\bullet}H$, $\equiv C\text{-}O^{\bullet}$, and $=CH\text{-}O^{\bullet}$ sites on the BDD surface. Chemisorption of the oxychlorine radicals stabilizes them and gives them a longer lifetime to react. This may explain the greater perchlorate generation observed with BDD anodes compared to platinum and metal oxide coated anodes (38). Activationless pathways involving surface reactions exist for producing $HClO_2$ and $HClO_3$. However, production of perchlorate or perchloric acid via chemisorbed

intermediates both require a substantial activation energy, consistent with this being the rate-limiting step between hypochlorite and perchlorate (37).

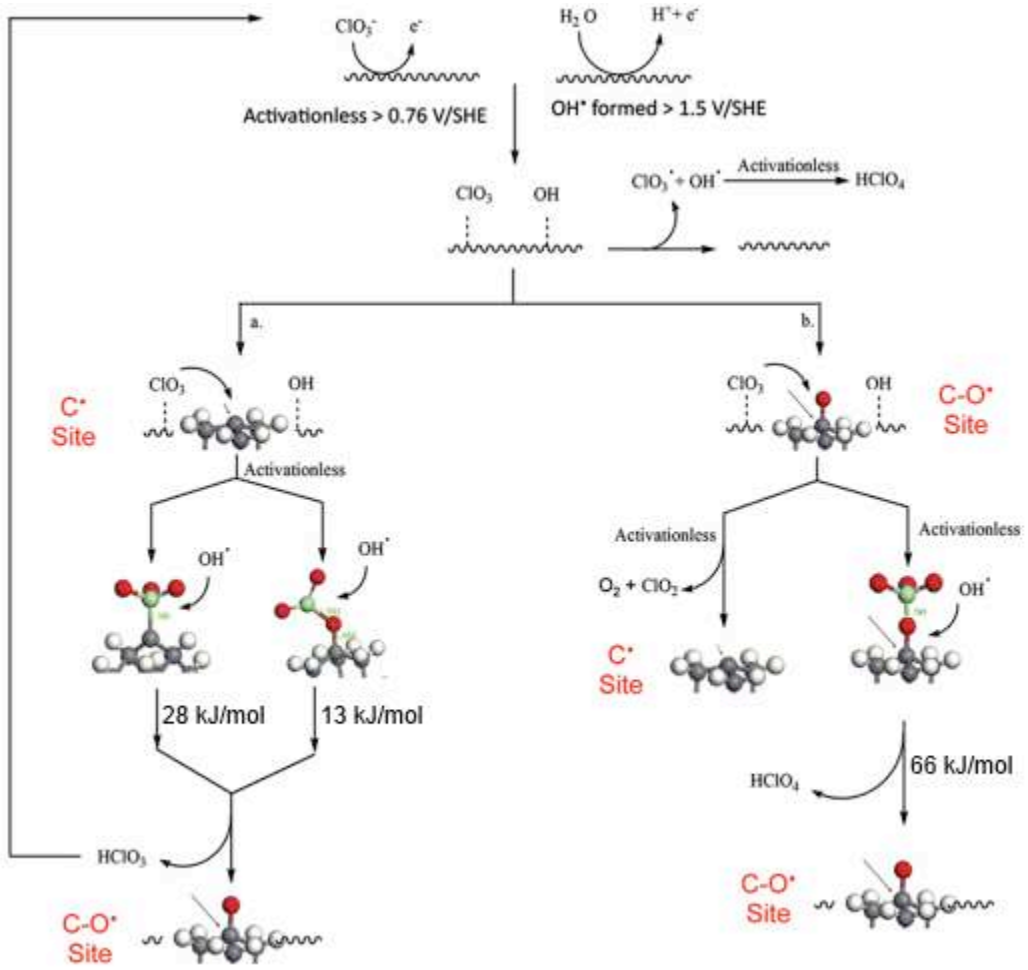

Figure 7. Schemes for formation of $HClO_3$ and $HClO_4$ from $ClO_3^{\bullet}$ on BDD anode surface. Atom key for electronic version of manuscript: carbon, grey; hydrogen, white; oxygen, red; chlorine, green.

Acknowledgments

Funding for this work was provided by the National Science Foundation (CBET-0931749).

References

1. H. B. Martin, A. Argotia, U. Landau, A. B. Anderson and J. C. Angus, *J. Electrochem. Soc.,* **143**, L133 (1996).
2. K. E. Carter and J. Farrell, *Environ. Sci. Technol*., **42**, 6111 (2008).
3. J. F. Zhi, H. B. Wang, T. Nakashima, T. N. Rao and A. Fujishima, *J. Phys. Chem. B,* **107**, 13389 (2003).
4. B. P. Chaplin, G. Schrader and J. Farrell, *Environ. Sci. Technol.,* **43**, 8302 (2009).
5. B. P. Chaplin, G. Schrader and J. Farrell, *Environ. Sci. Technol.,* **44**, 4264 (2010).
6. M. J. Pacheco, V. Santos, L. Ciriaco, and A. Lopes, *J. Hazard. Mater.,* **186**, 1033 (2011).

7. M. Mascia, A. Vacca, A. M. Polcaro, S. Palmas, J. R. Ruiz and A. Da Pozzo, *J. Hazard. Mater.,* **174**, 314 (2010).
8. M. E. H Bergmann, *Electrochemistry for the Environment*, C. Comninellis and G. Chen, Editors, p. 163, Springer, New York (2009).
9. M. E. H. Bergmann, J. Rollin and T. Iourtchouk, *Electrochimica Acta*, ***54***, 2102 (2009).
10. M. E. H. Bergmann and J. Rollin, *Catal. Today*, **124**, 198 (2007).
11. A. M. Polcaro, A. Vacca, M. Mascia, and F. Ferrara, *J. Appl. Electrochem*. **38**, 979 (2008).
12 A. M. Polcaro, A. Vacca, M. Mascia, S. Palmas and J. R. Ruiz, *J. Appl. Electrochem.* **39**, 2083 (2009).
13. E. T. Urbansky and M. R. Schock, *J. Environ. Man*., **56**, 79 (1999).
14. E.T. Urbansky, *Environ. Sci. Pollut. Res.,* **9**, 187 (2002).
15. G. Lang and G. Horanyi, *J. Electroanal. Chem.*, **552**, 197 (2003).
16. *Interim Drinking Water Health Advisory for Perchlorate*, **EPA 822-R-08-025**, U.S. Environmental Protection Agency, Washington, DC (2008).

17. *Perchlorate in Drinking Water*, **R-16-04**, California Department of Health Services, Sacramento, California (2007).
18. *Perchlorate Information*, Massachusetts Department of Environmental Protection, Boston, Massachusetts (2008).
19. J. S. Xu, M. C. Granger, Q. Y. Chen, J. W. Strojek, T. E. Lister and G. M. Swain, *Anal. Chem.,* **69**(19), A591 (1997).
20. H. A. Girard, N. Simon, D. Ballutaud, E. de La Rochefoucauld and A. Etcheberry, *Diamond and Related Materials,* **16**(4-7), 888 (2007).
21. K. B. Holt, A. J. Bard, Y. Show and G. M. Swain, *J. Phys. Chem. B,* **108**(39), 15117 (2004).
22. H. B. Martin, A. Argoitia, U. Landau, A. B. Anderson and J. C. Angus, *J. Electrochem. Soc.,* **143**(6), L133 (1996).
23. D. Mishra, Z. H. Liao and J. Farrell, *Environ. Sci. Technol.,* **42**, 9344 (2008).
24. B. P. Chaplin, D. K. Hubler and J. Farrell, *Electrochimica Acta*, **89**, 122 (2012).
25. Materials Studio, version 4.2, Accelrys Corporation, San Diego, CA (2007).
26. B. Delley, *J. Chem. Phys.,* **92**, 508 (1990).
27. B. Delley, *J. Chem. Phys.*, **113**, 7756 (2000).
28. B. Delley, *J. Phys. Chem.*, **100** 6107 (1996).
29. A. D. Becke, *Phys. Rev. A*, **38**, 3098 (1988).

30. C. T. Lee, W. T. Yang and R. G. Parr, *Phys. Rev. B*, **37**, 785 (1988).
31. B. Delley, *Phys. Rev. B*, **66**, 155125, 1 (2002).
32. B. Delley, *Mol. Simulat.*, **32**, 117 (2006).
33. S. P. de Visser, *J. Biocatal. Biotransformation*, **1**, 1 (2012).
34. A. B. Anderson and D. B. Kang, *J. Phys. Chem. A*, **102,** 5993 (1998).
35. Y. Cai, A. B. Anderson, J. C. Angus, and L. N. Kostadinov, *J. Electrochem. Soc.,* **154** F36 (2007).
36. C. P. Kelly, C. J. Cramer and D. G. Truhlar, *J. Phys. Chem. A*, **110**, 2493 (2006).
37. A. Orchideh, D. K. Hubler, G. Schrader, J. Farrell and B. P. Chaplin, *Environ. Sci. Technol.*, **45** 10582 (2011).
38. A. Kraft, *Platinum Metals Review*, **52**(3), 177 (2008).